Astron. Astrophys. 362, 410–418 (2000)

ASTRONOMY AND ASTROPHYSICS

The FERRUM project: new experimental and theoretical f-values for 4p-4d transitions in Fe II applied to HST spectra of χ Lupi

H. Nilsson[1], C.M. Sikström[1], Z.S. Li[2], H. Lundberg[2], A.J.J. Raassen[4], S. Johansson[1], D.S. Leckrone[3], and S. Svanberg[2]

[1] Atomic Spectroscopy, Department of Physics, University of Lund, P.O. Box 118, 221 00 Lund, Sweden (hampus.nilsson@fysik.lu.se)
[2] Department of Physics, Lund Institute of Technology, P.O. Box 118, 221 00 Lund, Sweden
[3] NASA/Goddard Space Flight Center, Code 630, Greenbelt, MD 20771, USA
[4] Astronomical Institute "Anton Pannekoek", University of Amsterdam, Kruislaan 403, 1098 SJ, Amsterdam, The Netherlands

Received 30 May 2000 / Accepted 8 August 2000

Abstract. Radiative lifetimes for six highly excited levels in Fe II have been measured at Lund Laser Centre applying the laser induced fluorescence technique and two-step excitation. The energy levels belong to the even-parity $3d^6(^5D)4d$ subconfiguration at about 10 eV. Branching fractions (BF:s) of 29 transitions from these levels to the $3d^6(^5D)4p$ subconfiguration at about 5 eV have been measured in the wavelength region 2000–3000 Å with the Lund Fourier Transform Spectrometer. By normalizing the BF:s with the lifetimes we get experimental oscillator strengths for these 29 4p-4d lines. The oscillator strengths are compared with new theoretical calculations using the orthogonal operator technique and applied to high-resolution spectra of the star χ Lupi, recorded with the *Hubble Space Telescope*.

Key words: atomic data – line: identification – methods: laboratory – ultraviolet: stars – stars: individual: χ Lupi

1. Introduction

The FERRUM project is an international collaboration (project leader: S. Johansson, Lund University) aiming at extending and improving the database of Fe II oscillator strengths by combining experimental, observational and theoretical data. The experimental f-values are produced by combining radiative lifetimes, measured at the Lund Laser Centre, with branching fractions, measured in laboratory emission spectra using the Fourier Transform Spectrometer (FTS) at Lund University. The observational data are derived from stellar photospheric spectra primarily obtained with the *Hubble Space Telescope* (HST) and the Nordic Optical Telescope (NOT). The theoretical data are calculated by one of the authors using the orthogonal operator technique. The scientific goal of the FERRUM project is to produce two sets of f-values - one for optical and one for ultraviolet stellar spectroscopy- covering a wide range in excitation potential (EP).

The high cosmic abundance of iron permits weak lines of Fe II to be observed in spectra of stars at temperatures favoring the first ionization stage. Weak lines could be associated with a combination of either (low EP)·(low f-value) or (high EP)·(high f-value), where the EP refers to the lower level of a transition. One way to study high excitation lines in Fe II is thus to look for intrinsically strong transitions. There is an advantage to use transitions, for which the upper level has the same parity as the ground configuration. Such levels decay to levels of opposite parity, which are not metastable, and the lines are therefore not subject to self absorption. So far, no experimental data have been available for such Fe II transitions.

In previous papers within the FERRUM project we have described the procedure for measuring radiative lifetimes of high 4p states in Fe II using the LIF technique, where the laser excitation has to take place from a high metastable state (Li et al. 1999, hereafter Paper I). In a second paper we have measured experimental oscillator strengths for 18 UV lines of Fe II, also from high 4p states (Sikström et al. 1999). In the present paper we present the first measurements of radiative lifetimes of six levels of the $3d^6(^5D)4d$ subconfiguration, having the same parity as the ground state of Fe II. By measuring the branching fractions of these levels we can present the first experimental f-values for twenty-nine 4p-4d transitions, all of them appearing in the satellite UV region. Eight of these lines seem to be unblended in the spectra of χ Lupi recorded with the Goddard High Resolution Spectrograph (GHRS) previously on board the *Hubble Space Telescope* (HST) (Leckrone et al. 1999, Brandt et al. 1999).

2. Lifetime measurements

The radiative lifetimes of six $3d^6(^5D)4d$ levels, $^4G_{11/2}$, $^4G_{9/2}$, $^4D_{7/2}$, $^6D_{9/2}$, $^6D_{7/2}$, and $^6P_{7/2}$, were measured using the method of laser induced fluorescence (LIF). The experiment involved three Nd:YAG lasers, two tunable dye lasers and a Brillouin scattering cell for laser pulse shortening (see Fig. 1 and Paper I for details). The measured $3d^64d$ levels have energies around 10 eV and the same parity (even) as the ground configuration $3d^64s$. This means that the 4d-levels must be excited either in one step by a two-photon process or in two steps via the odd-parity $3d^64p$ configuration. We have investigated both methods.

Send offprint requests to: H. Nilsson

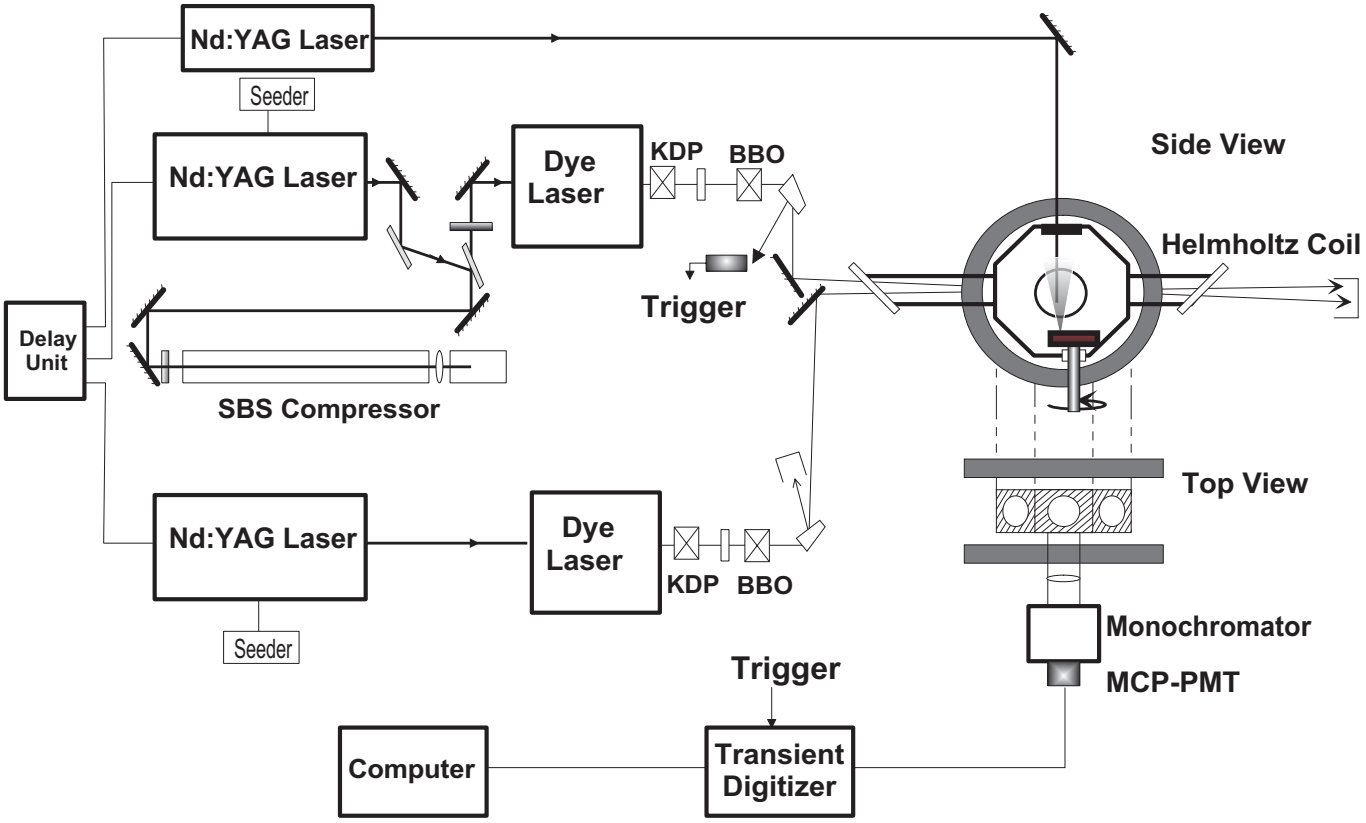

Fig. 1. Experimental setup for lifetime measurements.

2.1. Methods

A laser induced plasma was used as an ion source. The frequency doubled radiation from a Nd:YAG laser was focused onto a rotating iron target, producing an expanding plasma through ablation that contains free atoms and ions of different degrees of ionization in the ground state as well as in metastable states. (As the Fe^+-ions were excited from the ground state a later part of the expanding plasma cone could be used, in which most of the Fe^+-ions have decayed to the ground state.) The excitation beams were directed to cross the plasma about 1 cm above the ablation point. The plasma background radiation at this position was negligible.

In Fig. 2 the two-photon excitation and the two-step excitation processes are illustrated. When using two-photon excitation, the photon energy was matched to half the energy difference between the lower and upper level. A virtual level is formed half-way between the two levels, enabling the transition to take place. The probability for this process is increased if there is a real level of opposite parity close to the virtual level. In the present case it was possible to start from the ground state, and thus the energy of the laser was tuned to half the excitation energy of the upper level. Since the process involves two photons with the same energy, only one tunable laser is needed to reach levels with the same parity as the ground state. The process of two photon-excitation is a non-linear effect, and therefore the intensity of the laser radiation must be high. That can be achieved by focusing the laser beam, but this will give a small interaction volume and a low number of activated ions, and hence weak fluorescence signals.

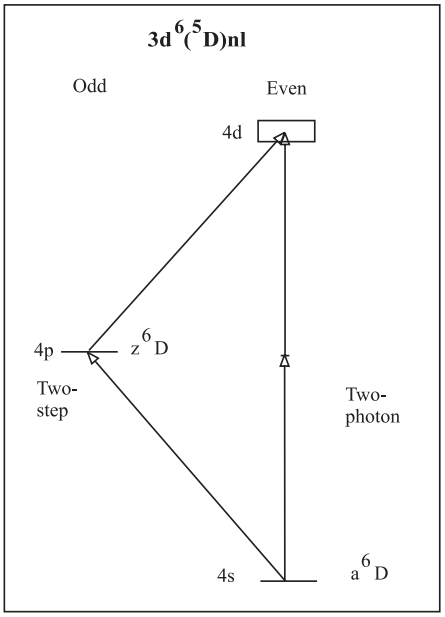

Fig. 2. Scheme of the two-step and the two-photon excitation routes from the ground state $3d^6 4s\ a^6D_{9/2}$ to the 4d levels in Fe II.

In a two-step excitation, a real intermediate level of opposite parity is used. Two lasers must be tuned to match the

wavelengths of the two excitations (Fig. 2), and have both spatial and temporal overlap. In this case there is no need to focus the beams since the laser radiation was strong enough to saturate both transitions. Both methods described here were tested, and we found the results from the two-step excitation to be the most reliable. Thus, the results presented are exclusively from two-step LIF signals, described in more detail below.

2.2. Experiment

The investigated levels (Table 1), were excited with the two-step technique. In the first excitation step Fe^+-ions were transferred from the ground state to an intermediate odd $3d^6 4p$ level at roughly 5 eV. Since the ground state of Fe II is $3d^6(^5D)4s\ a^6D_{9/2}$ we chose $3d^6(^5D)4p\ z^6D_{9/2}$ as the intermediate level for all the 4d levels investigated. It is located at 38459 cm^{-1}, and is the lowest odd-parity level in Fe II. Using the ground state for the first step excitation has two major advantages. Firstly, the population in the ground state is about one order of magnitude higher than in a low metastable state. The fluorescence signal will be larger in the same proportion, as we get a higher population in the intermediate $z^6D_{9/2}$ level. Secondly, it is possible to use a later part of the expanding plasma, where the plasma background and the influence of collisions in the plasma are negligible.

For the first step, the frequency doubled output (532 nm) of a Nd:YAG laser was used to pump a dye laser, producing near-infrared laser pulses, at a repetition rate of 10 Hz. The dye laser was tuned to 779.9 nm and the output frequency doubled in a KDP crystal. After matching the polarization of the first and second harmonics of the dye laser the two wavelengths were mixed in a BBO crystal, producing the third harmonic. The three wavelengths were separated in a prism, and only the frequency tripled radiation was sent to the target chamber. This provided 8 ns long laser pulses at the desired wavelength, 260.0 nm.

The second step excitation required laser pulses between 205 and 220 nm to cover the excitation of various 4d levels, and with a time duration shorter than the lifetimes to be measured. The pulses from a second Nd:YAG laser were frequency doubled and compressed in time using Stimulated Brillouin Scattering (SBS) in a water cell. The pulses were compressed from 8 ns to roughly 1 ns (FWHM). A more detailed description of this technique can be found in Li et al. (1999). The compressed pulse was then used to pump a dye laser, providing tunable radiation in the range 615–660 nm. This radiation was frequency tripled giving excitation wavelengths at 205–220 nm, which match the wavelengths of the 4p-4d transitions. The radiation was separated using the same scheme as with the first step excitation pulse. The first and second step laser excitation pulses were spatially combined in the target chamber.

The LIF signal was detected in a direction perpendicular to the ablation laser beam as well as to the two excitation beams. The signal was focused by a fused-silica lens onto the entrance slit of a 1/8 m monochromator (6.4 nm/mm resolution) and detected by a photo-multiplier tube (PMT) with a rise time of 200 ps. Only relatively weak signals were recorded to keep the PMT working in the linear region. A decay channel different from the excitation was used to detect the LIF. The signal was sent to a digital transient recorder with 1 GHz bandwidth and a real time sampling rate of 2 GS/s. The second step laser pulse was used to trigger the oscilloscope. 1000 pulses were averaged to develop the exponential decay curve. The averaged time-resolved LIF decay curves were transferred to a PC where the evaluation was done immediately. LIF signals from both the first and second step were recorded. The influence of background light from the decay of the intermediate level was carefully checked. Saturation of the second step was checked and avoided by inserting a suitable number of neutral density filters into the second step laser beam.

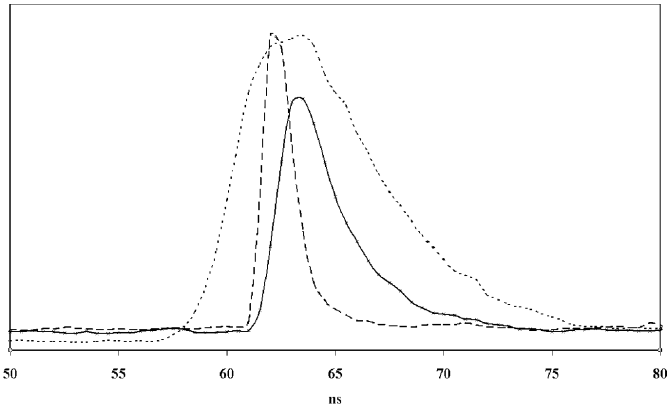

Fig. 3. An illustration of the position of the two excitation pulses in time. The dotted curve shows the fluorescence signal following the first excitation step, and the dashed curve is the second step excitation pulse (FWHM≈1.5 ns). The solid curve shows the fluorescence signal following the second step.

Two trigger boxes were used to synchronize the three laser pulses. Trigger pulses controlled both the flash lamps of the three Nd:YAG lasers as well as the Q-switches. The positioning in time of the three pulses can in some cases have an effect on the measured lifetime. If the two excitation pulses cross the plasma too early, collisions in the plasma could shorten the measured lifetime. Another problem was the positioning of the two excitation pulses relative to each other. It was important to have the second step laser pulse arrive in the saturated part of the first step excitation to eliminate the effect of decay of the intermediate level entering into the LIF decay curve from the second step. The correctness of the relative position of the two pulses was checked by moving the second pulse in time and recording and evaluating LIF curves at different positions in time. A clear trend could be found, as well as a change in the shape of the LIF curves. In general, positioning the second step pulse before saturation gave longer lifetimes and decay curves, which, as expected, could not be evaluated with a single decay. Positioning the pulse after the saturated part did not have as large of an influence either on the LIF decay curve or on the evaluated lifetime as if positioned too early. This is illustrated in Fig. 3.

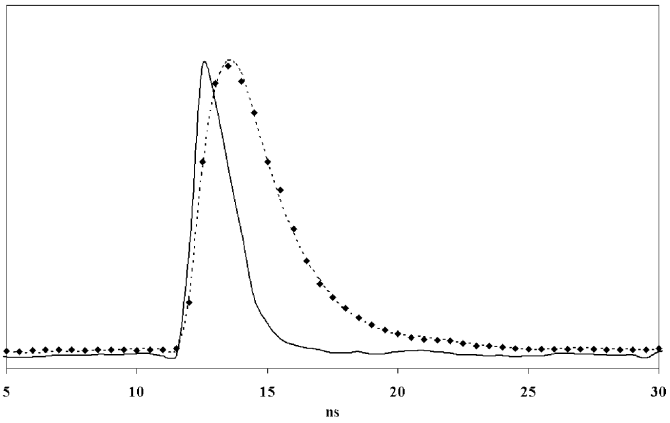

Fig. 4. The curve shows the decay from the $^4D_{7/2}$ level. The solid curve shows the recorded second step excitation pulse and the dashed line the fitted LIF curve. The recorded data points of the LIF are marked as $\diamond$ in the figure. The lifetime obtained from this particular curve is 1.85 ns.

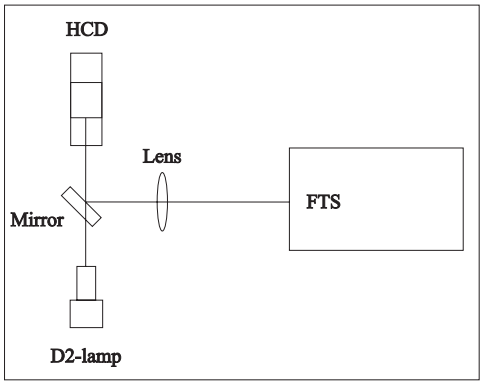

Fig. 5. The experimental setup with the HCD, D_2-lamp, turnable mirror and FT-spectrometer.

The lifetimes were evaluated by a least-squares fit of a convolution of the recorded laser excitation pulse and an exponential decay curve to the recorded fluorescence signal. An example of a recording is shown in Fig. 4. On average, about 20 recordings were used to evaluate each lifetime. The results for the six levels measured are given in Table 1. Three of them belong to two different quartet terms (^{4}G and ^{4}D) and the other three are sextet levels (^{6}D and ^{6}P). Levels belonging to the same LS term were found to have the same lifetime. The sextet levels have slightly shorter lifetimes than the quartet levels, which may be partly explained by additional deexcitation channels. The uncertainties given include statistical errors as well as the systematic errors discussed above. The statistical spread obtained for different runs is typically ± 0.05 ns.

3. Branching fractions

The branching fraction (BF) is defined as the transition probability of a single line divided by the sum of all transition probabilities from the same upper level. Since the measured intensity of a line is proportional to the transition probability, it is possible to derive experimental BF:s. This requires that the intensities are corrected for wavelength dependence and that all transitions from the upper level, or at least the prominent ones, can be measured.

The spectrum from an iron hollow cathode discharge (HCD) lamp, run in a mixture of argon and neon at a pressure of one torr, was recorded with a Fourier transform spectrometer (FTS). The FTS has different response at different wavelengths (due to e.g. detectors and optics), and it is necessary to calibrate the measured intensities. This was done with a deuterium (D_2) lamp giving a continuous spectrum with a known spectral intensity distribution. The experiment was set up as a T (Fig. 5) with a movable mirror in the center of the T, making it possible to switch between the two light sources without moving them. It is crucial to place the light sources at the same distance from the FTS aperture so that the optical paths are equivalent. The spectrum of the D_2 lamp was recorded before and after each run with the HCD, and an average of the calibration spectra was used to correct for the instrument response. The D_2 lamp has been calibrated at the Physikalisch-Technische Bundesanstalt, Berlin, Germany, to a 2 σ accuracy of 8% in the spectral region 33000–60000 cm^{-1}. The calibration was independently checked against Ar II lines with known branching ratios (Siems et al. 1995), and an agreement within 10% was found.

FTS spectra were recorded in the region 33000–50000 cm^{-1} (3000–2000 Å) with different currents through the HCD in order to check for possible effects of self absorption. As expected we found no indication of self absorbtion in the 4p-4d lines, because the 4p levels have short lifetimes and fast decay channels. The 4d levels studied have no strong branches outside the recorded wavelength interval, which reduces the uncertainties in the BF measurements. The interferogram recorded with the FTS was transformed with the help of a computer code, GREMLIN, a development of DECOMP (Brault & Abrams 1989). A Voigt profile was fitted to the recorded line, and the area of the Voigt profile was taken as a measure of the intensity. Transitions having a BF smaller than 1% could not be seen in the spectrum. The total intensity of the unobserved transitions from a given upper level is called the residual and must be taken into account in the evaluation. This was done by using theoretical values from our calculations. Since the residual is only a few percent for each level, the uncertainty introduced by using calculations is small compared with the other uncertainties. The largest error in the BF is due to the intensity calibration. The uncertainty associated with the fitting procedure is related to the signal to noise ratio (S/N) of the individual lines. These uncertainties were estimated with the help of a computer code (Blom 2000), which calculates the standard deviation when fitting a gaussian to a line of given S/N. The uncertainty in the BF:s is less than 8 % and depends on the S/N of the line. The uncertainty in the calibration lamp used is set to 4% (1 σ), and the uncertainty in determining the instrument response is estimated to 10%.

Table 1. Experimental and theoretical lifetimes of six 4d levels in Fe II

Config.	Term	J	E	Exc. (2^{nd} step)	Fluorescence	Lifetime (ns)	
			(cm^{-1})	λ_{air}(nm)	λ_{air}(nm)	Exp.	Theory
$3d^6$ (^{5}D) 4d	^{4} G	11/2	84863.38	215.4	246.0	1.8 (2)	1.8
$3d^6$ (^{5}D) 4d	^{4} G	9/2	85184.77	214.0	247.2	1.8 (2)	1.8
$3d^6$ (^{5}D) 4d	^{4} D	7/2	84685.24	216.3	248.4	1.9 (2)	1.8
$3d^6$ (^{5}D) 4d	^{6} D	9/2	83726.41	220.8	243.4	1.7 (2)	1.5
$3d^6$ (^{5}D) 4d	^{6} D	7/2	83713.57	220.9	243.5	1.7 (2)	1.5
$3d^6$ (^{5}D) 4d	^{6} P	7/2	84266.59	218.2	243.7	1.75 (20)	1.6

4. Oscillator strengths

In Table 2 we list all the 29 transitions from the six 4d levels, for which we have experimental lifetimes and branching fractions. For each line we give the upper and lower levels, air wavelength as well as vacuum wavelength. Column 5 lists the measured branching fractions. The tabulated log gf-values are the experimental values from the present work (Exp.), the calculated values from Raassen (Calc.), data from the Kurucz database (Kurucz 1993), and finally we give a relative uncertainty of each experimental gf-value. The data are discussed below.

In Table 3 we present a finding list of all lines originating from the six measured 4d levels for which the theoretical log gf-values ≥ -3. This is justified by the good agreement between experimental and calculated values, and the potential needs for weak lines in abundance analyses. We also include the experimental values for the 29 measured lines. In Column 6 we give astrophysical log gf-values derived from the GHRS spectrum of χ Lupi (see below).

4.1. Experimental data

By combining the branching fractions with the lifetime measurements in Table 1 we have derived the Einstein coefficients A, and converted them into oscillator strengths (f) using a standard formula. To meet the astrophysical needs we present the data as log gf-values. The uncertainty of the experimental log gf-values depends on the uncertainty in the measured lifetime, given in Table 1, and the uncertainty in the branching fraction, discussed in Sect. 3. The final uncertainties in Table 2, derived by inserting all contributions into an error of propagation formula, are probably conservative estimates. The residuals in Table 2 take care of the unobserved branches from each upper level, and they are in most cases only a few percent.

4.2. Theoretical data

The theoretical data presented in Tables 2 and 3 are based on calculations using the orthogonal operator technique (Raassen & Uylings 1998a,b). The orthogonal operator technique is a semi-empirical method, like the Cowan code method, and it can be seen as a next step in the semi-empirical description of complex spectra. By orthogonalization of the operators, the least squares fit of model Hamiltonian eigenvalues to experimental energy levels is optimized, which means that the parameters are as independent and stable as possible (Hansen et al. 1988). As a result several smaller thus far neglected higher order or relativistic effects can meaningfully be added. The introduction of these effects results in a better description of the energy level structure (the eigenvalues), and thereby a better description of the eigenvector compositions. This is essential when doing a detailed study of a complex spectrum which has many closely lying energy levels. However, a fairly accurate ab-initio calculation to provide starting parameter values for the higher order magnetic interactions has to precede the fitting procedure. For this ab-initio calculation we used a relativistic Hartree-Fock program (MCDF from Parpia et al. 1996). The eigenvector compositions obtained in this way were used to transform the pure LS transition matrix into the realistic intermediate coupling situation. The transition integrals were calculated using the MCDF program of Parpia et al. and corrected for core polarization (Hameed 1972; Laughlin 1992). The latter resulted in a decrease in about 5–10% of the values obtained from the MCDF program.

The theoretical data in the present paper are, together with other atomic data, available on the internet site:
http://www.wins.uva.nl/research/atom/levtext.html.
The data can also be downloaded via ftp:
ftp://ftp.wins.uva.nl/pub/orth.

4.3. Astrophysical data

The 4p-4d transitions discussed in this paper appear in a limited wavelength region between 2000 and 2500 Å. Short wavelength intervals in this region, 10–12 Å each, have been recorded of the chemically peculiar star χ Lupi using the Goddard High Resolution Spectrograph (GHRS) previously on board the *Hubble Space Telescope* (HST) (Brandt et al. 1999). Even though the star has a line rich spectrum, due to its chemical composition, it is still a most useful target in the ultraviolet region to test atomic parameters. The star has a suitable temperature ($T_{\rm eff}$=10650 K) for producing strong lines of the second spectrum, and the lines are narrow due to a very small rotational velocity and a low photospheric turbulence. The star is a binary system, and one has to be careful with the contribution from the secondary star to the spectrum. We have used the GHRS observations and the synthetic spectra of χ Lupi in the relevant

Table 2. Experimental gf-values of Fe II, derived from measured branching fractions (BF:s) and the lifetimes in Table 1, compared with theoretical data.

Level		Wavelength[a]		BF	log *gf*			Unc.[b]
upper	lower	air (Å)	vac (Å)		Exp.	Calc.	Kurucz	
4d ^{6}D$_{7/2}$	4p z^{6}P$_{7/2}$	2434.999	2435.737	0.343	+0.157	+0.202	+0.212	15
	4p z^{6}F$_{7/2}$	2410.270	2411.003	0.130	−0.273	−0.282	−0.297	16
	4p z^{6}D$_{5/2}$	2228.732	2229.425	0.271	−0.022	+0.014	+0.004	15
	4p z^{6}D$_{9/2}$	2209.032	2209.721	0.217	−0.127	−0.056	−0.058	16
	residual			0.039				
4d ^{6}D$_{9/2}$	4p z^{6}P$_{7/2}$	2434.238	2434.976	0.343	+0.253	+0.286	+0.240	15
	4p z^{6}F$_{9/2}$	2402.446	2403.177	0.099	−0.298	−0.232	−0.323	17
	4p z^{6}F$_{11/2}$	2394.002	2394.731	0.016	−1.092	−1.045	−1.078	19
	4p z^{6}D$_{7/2}$	2218.259	2218.950	0.267	+0.064	+0.123	+0.140	15
	4p z^{6}D$_{9/2}$	2208.406	2209.094	0.271	+0.067	+0.104	+0.130	15
	residual			0.004				
4d ^{6}P$_{7/2}$	4p z^{4}P$_{5/2}$	2680.232	2681.029	0.019	−1.022	−1.039	−0.893	19
	4p z^{4}D$_{7/2}$	2510.565	2511.321	0.027	−0.934	−0.946	−0.760	18
	4p z^{6}P$_{5/2}$	2436.622	2437.361	0.473	+0.284	+0.308	+0.299	13
	4p z^{6}P$_{7/2}$	2402.633	2403.364	0.144	−0.246	−0.283	−0.333	16
	4p z^{6}F$_{7/2}$	2378.554	2379.279	0.030	−0.938	−0.902	−0.837	18
	4p z^{6}D$_{5/2}$	2201.586	2202.274	0.136	−0.345	−0.234	−0.228	16
	4p z^{6}D$_{7/2}$	2191.983	2192.668	0.132	−0.362	−0.286	−0.296	16
	4p z^{6}D$_{9/2}$	2182.361	2183.044	0.015	−1.306	−1.290	−1.389	21
	residual			0.024				
4d f^{4}D$_{7/2}$	4p z^{4}P$_{5/2}$	2650.481	2651.270	0.305	+0.131	+0.136	+0.120[c]	13
	4p z^{4}F$_{7/2}$	2503.539	2504.293	0.063	−0.602	−0.550	−0.813	15
	4p z^{4}D$_{7/2}$	2484.442	2485.192	0.411	+0.205	+0.232	+0.230	12
	4p z^{4}F$_{9/2}$	2471.276	2472.023	0.079	−0.517	−0.533	−0.500	15
	4p z^{6}P$_{5/2}$	2412.008	2412.741	0.032	−0.936	−0.886	−0.711	16
	4p z^{6}P$_{7/2}$	2378.697	2379.423	0.028	−0.994	−0.881	−0.778	16
	4p z^{6}F$_{5/2}$	2360.531	2361.253	0.042	−0.828	−0.931	−1.276	16
	residual			0.040				
4d e^{4}G$_{9/2}$	4p z^{4}F$_{7/2}$	2472.605	2473.353	0.580	+0.470	+0.475	+0.530	13
	4p z^{4}D$_{7/2}$	2453.976	2454.719	0.236	+0.073	+0.097	−0.180	16
	4p z^{4}F$_{9/2}$	2441.129	2441.869	0.161	−0.097	−0.097	−0.122	16
	residual			0.023				
4d e^{4}G$_{11/2}$	4p z^{4}F$_{9/2}$	2460.440	2461.185	0.972	+0.769	+0.779	+0.760	12
	4p z^{6}F$_{9/2}$	2338.544	2339.261	0.010	−1.262	−1.086	−1.274	22
	residual			0.018				

[a] Preliminary Ritz wavelengths from current work on Fe II in Lund.
[b] Uncertainty in the f-value in %.
[c] Also included in the NIST compilation by Fuhr et al. (1988).

intervals to extract information about the 4p-4d transitions. The model atmospheres used were the ATLAS8 models described by Wahlgren et al. (1994). The synthetic spectra were calculated with SYNTHE and the Kurucz line lists (1993). Using the iron abundance adopted for the star (Leckrone et al. 1999) we have adjusted the log gf-values in the calculated spectrum to match the observed line widths of unblended features that correspond to 4p-4d transitions in Table 3. In Fig. 6 we illustrate the fitting procedure with two of the stellar lines at 2208.4 and 2209.0 Å. It is not clear why strong lines show a disagreement in the central absorption of the calculated and the observed lines. The uncertainty of the astrophysical log gf-values associated with the fitting procedure varies for individual lines due to the depth and shape of the observed line profile. The uncertainty also depends on probable blends in the observed feature, and we can therefore only set an upper limit of the log gf values. A measure of this uncertain uncertainty is the scatter in the discrepancy between astrophysical and laboratory log gf-values.

5. Discussion

In Figs. 7 - 8 we show comparisons between our experimental data and the two sets of theoretical data by plotting the difference in log gf as a function of log gf for both theoretical data sets. In Fig. 7 the comparison between the experimental and theoretical data reported in this paper shows a remarkably good agreement. There is a good reason to believe that also the calculated values for other transitions of the (^5D)4p-(^5D)4d transition array, not

Table 3. Finding list for downward transitions from the measured $3d^6 4d$ levels having $\log gf \geq -3$.

Wavelength[a]	Level		log gf		
air (Å)	upper	lower	Calc.	Exp.	χ Lupi[b]
2139.472	$3d^6\ 4d\ {}^4G_{9/2}$	$3d^6\ ({}^5D)\ 4p\ z^6D_{9/2}$	−2.763		−2.85
2148.719	$3d^6\ 4d\ {}^4G_{9/2}$	$3d^6\ ({}^5D)\ 4p\ z^6D_{7/2}$	−2.414		*bl*
2154.291	$3d^6\ 4d\ {}^4G_{11/2}$	$3d^6\ ({}^5D)\ 4p\ z^6D_{9/2}$	−1.663		*bl*
2162.594	$3d^6\ 4d\ {}^4D_{7/2}$	$3d^6\ ({}^5D)\ 4p\ z^6D_{9/2}$	−2.254		
2172.042	$3d^6\ 4d\ {}^4D_{7/2}$	$3d^6\ ({}^5D)\ 4p\ z^6D_{7/2}$	−1.546		
2181.471	$3d^6\ 4d\ {}^4D_{7/2}$	$3d^6\ ({}^5D)\ 4p\ z^6D_{5/2}$	−2.417		
2182.361	$3d^6\ 4d\ {}^6P_{7/2}$	$3d^6\ ({}^5D)\ 4p\ z^6D_{9/2}$	−1.290	−1.306	
2191.983	$3d^6\ 4d\ {}^6P_{7/2}$	$3d^6\ ({}^5D)\ 4p\ z^6D_{7/2}$	−0.286	−0.362	
2201.586	$3d^6\ 4d\ {}^6P_{7/2}$	$3d^6\ ({}^5D)\ 4p\ z^6D_{5/2}$	−0.234	−0.345	−0.10
2208.406	$3d^6\ 4d\ {}^6D_{9/2}$	$3d^6\ ({}^5D)\ 4p\ z^6D_{9/2}$	+0.104	+0.067	+0.50
2209.032	$3d^6\ 4d\ {}^6D_{7/2}$	$3d^6\ ({}^5D)\ 4p\ z^6D_{9/2}$	−0.056	−0.127	+0.30
2218.259	$3d^6\ 4d\ {}^6D_{9/2}$	$3d^6\ ({}^5D)\ 4p\ z^6D_{7/2}$	+0.123	+0.064	
2218.891	$3d^6\ 4d\ {}^6D_{7/2}$	$3d^6\ ({}^5D)\ 4p\ z^6D_{7/2}$	−1.961		
2228.732	$3d^6\ 4d\ {}^6D_{7/2}$	$3d^6\ ({}^5D)\ 4p\ z^6D_{5/2}$	+0.014	−0.022	
2321.092	$3d^6\ 4d\ {}^4G_{9/2}$	$3d^6\ ({}^5D)\ 4p\ z^6F_{9/2}$	−2.194		
2327.698	$3d^6\ 4d\ {}^4G_{9/2}$	$3d^6\ ({}^5D)\ 4p\ z^6F_{7/2}$	−1.300		*bl*
2330.542	$3d^6\ 4d\ {}^4G_{11/2}$	$3d^6\ ({}^5D)\ 4p\ z^6F_{11/2}$	−1.618		−1.75
2338.544	$3d^6\ 4d\ {}^4G_{11/2}$	$3d^6\ ({}^5D)\ 4p\ z^6F_{9/2}$	−1.086	−1.262	−1.05
2348.331	$3d^6\ 4d\ {}^4D_{7/2}$	$3d^6\ ({}^5D)\ 4p\ z^6F_{9/2}$	−2.720		*bl*
2355.093	$3d^6\ 4d\ {}^4D_{7/2}$	$3d^6\ ({}^5D)\ 4p\ z^6F_{7/2}$	−2.073		−1.96
2360.531	$3d^6\ 4d\ {}^4D_{7/2}$	$3d^6\ ({}^5D)\ 4p\ z^6F_{5/2}$	−0.931	−0.828	
2371.656	$3d^6\ 4d\ {}^6P_{7/2}$	$3d^6\ ({}^5D)\ 4p\ z^6F_{9/2}$	−1.486		
2378.554	$3d^6\ 4d\ {}^6P_{7/2}$	$3d^6\ ({}^5D)\ 4p\ z^6F_{7/2}$	−0.902	−0.938	*bl*
2378.697	$3d^6\ 4d\ {}^4D_{7/2}$	$3d^6\ ({}^5D)\ 4p\ z^6P_{7/2}$	−0.881	−0.994	*bl*
2384.101	$3d^6\ 4d\ {}^6P_{7/2}$	$3d^6\ ({}^5D)\ 4p\ z^6F_{5/2}$	−2.284		−2.46
2394.002	$3d^6\ 4d\ {}^6D_{9/2}$	$3d^6\ ({}^5D)\ 4p\ z^6F_{11/2}$	−1.045	−1.092	
2402.446	$3d^6\ 4d\ {}^6D_{9/2}$	$3d^6\ ({}^5D)\ 4p\ z^6F_{9/2}$	−0.232	−0.298	
2402.633	$3d^6\ 4d\ {}^6P_{7/2}$	$3d^6\ ({}^5D)\ 4p\ z^6P_{7/2}$	−0.283	−0.246	
2403.187	$3d^6\ 4d\ {}^6D_{7/2}$	$3d^6\ ({}^5D)\ 4p\ z^6F_{9/2}$	−2.385		
2409.524	$3d^6\ 4d\ {}^6D_{9/2}$	$3d^6\ ({}^5D)\ 4p\ z^6F_{7/2}$	−2.415		*bl*
2410.270	$3d^6\ 4d\ {}^6D_{7/2}$	$3d^6\ ({}^5D)\ 4p\ z^6F_{7/2}$	−0.282	−0.273	*bl*
2412.008	$3d^6\ 4d\ {}^4D_{7/2}$	$3d^6\ ({}^5D)\ 4p\ z^6P_{5/2}$	−0.886	−0.936	−0.90
2415.966	$3d^6\ 4d\ {}^6D_{7/2}$	$3d^6\ ({}^5D)\ 4p\ z^6F_{5/2}$	−1.152		−1.20
2434.238	$3d^6\ 4d\ {}^6D_{9/2}$	$3d^6\ ({}^5D)\ 4p\ z^6P_{7/2}$	+0.286	+0.253	
2434.999	$3d^6\ 4d\ {}^6D_{7/2}$	$3d^6\ ({}^5D)\ 4p\ z^6P_{7/2}$	+0.202	+0.157	+0.70
2436.622	$3d^6\ 4d\ {}^6P_{7/2}$	$3d^6\ ({}^5D)\ 4p\ z^6P_{5/2}$	+0.308	+0.284	*bl*
2441.129	$3d^6\ 4d\ {}^4G_{9/2}$	$3d^6\ ({}^5D)\ 4p\ z^4F_{9/2}$	−0.097	−0.097	+0.40
2453.976	$3d^6\ 4d\ {}^4G_{9/2}$	$3d^6\ ({}^5D)\ 4p\ z^4D_{7/2}$	+0.097	+0.073	
2460.440	$3d^6\ 4d\ {}^4G_{11/2}$	$3d^6\ ({}^5D)\ 4p\ z^4F_{9/2}$	+0.779	+0.769	
2469.916	$3d^6\ 4d\ {}^6D_{7/2}$	$3d^6\ ({}^5D)\ 4p\ z^6P_{5/2}$	−1.913		
2471.276	$3d^6\ 4d\ {}^4D_{7/2}$	$3d^6\ ({}^5D)\ 4p\ z^4F_{9/2}$	−0.533	−0.517	
2472.605	$3d^6\ 4d\ {}^4G_{9/2}$	$3d^6\ ({}^5D)\ 4p\ z^4F_{7/2}$	+0.475	+0.470	
2484.442	$3d^6\ 4d\ {}^4D_{7/2}$	$3d^6\ ({}^5D)\ 4p\ z^4D_{7/2}$	+0.232	+0.205	
2497.121	$3d^6\ 4d\ {}^6P_{7/2}$	$3d^6\ ({}^5D)\ 4p\ z^4F_{9/2}$	−1.940		
2503.539	$3d^6\ 4d\ {}^4D_{7/2}$	$3d^6\ ({}^5D)\ 4p\ z^4F_{7/2}$	−0.550	−0.602	
2510.565	$3d^6\ 4d\ {}^6P_{7/2}$	$3d^6\ ({}^5D)\ 4p\ z^4D_{7/2}$	−0.946	−0.934	
2524.153	$3d^6\ 4d\ {}^4D_{7/2}$	$3d^6\ ({}^5D)\ 4p\ z^4F_{5/2}$	−1.751		
2530.067	$3d^6\ 4d\ {}^6P_{7/2}$	$3d^6\ ({}^5D)\ 4p\ z^4F_{7/2}$	−1.752		*bl*
2532.051	$3d^6\ 4d\ {}^6P_{7/2}$	$3d^6\ ({}^5D)\ 4p\ z^4D_{5/2}$	−1.683		−1.80
2532.100	$3d^6\ 4d\ {}^6D_{7/2}$	$3d^6\ ({}^5D)\ 4p\ z^4F_{9/2}$	−2.541		−2.70
2545.093	$3d^6\ 4d\ {}^6D_{9/2}$	$3d^6\ ({}^5D)\ 4p\ z^4D_{7/2}$	−1.699		
2545.925	$3d^6\ 4d\ {}^6D_{7/2}$	$3d^6\ ({}^5D)\ 4p\ z^4D_{7/2}$	−1.415		
2551.122	$3d^6\ 4d\ {}^6P_{7/2}$	$3d^6\ ({}^5D)\ 4p\ z^4F_{5/2}$	−2.547		
2565.137	$3d^6\ 4d\ {}^6D_{9/2}$	$3d^6\ ({}^5D)\ 4p\ z^4F_{7/2}$	−2.442		

[a] Preliminary Ritz wavelengths from current work on Fe II in Lund.

[b] *bl* = line blended in the stellar spectrum; no entry = wavelength not covered by our HST observations.

Table 3. (continued)

Wavelength	Level		log gf		
air (Å)	upper	lower	Calc.	Exp.	χ Lupi
2565.982	$3d^6\ 4d\ ^6D_{7/2}$	$3d^6\ (^5D)\ 4p\ z^4F_{7/2}$	−1.751		
2650.481	$3d^6\ 4d\ ^4D_{7/2}$	$3d^6\ (^5D)\ 4p\ z^4P_{5/2}$	+0.136	+0.131	
2680.232	$3d^6\ 4d\ ^6P_{7/2}$	$3d^6\ (^5D)\ 4p\ z^4P_{5/2}$	−1.039	−1.022	−0.62
2720.571	$3d^6\ 4d\ ^6D_{7/2}$	$3d^6\ (^5D)\ 4p\ z^4P_{5/2}$	−2.583		
4116.962	$3d^6\ 4d\ ^4D_{7/2}$	$3d^6\ (a^3P)\ 4p\ y^4P_{5/2}$	−2.993		
4126.294	$3d^6\ 4d\ ^4G_{9/2}$	$3d^6\ (^3H)\ 4p\ z^4G_{7/2}$	−2.881		
4155.772	$3d^6\ 4d\ ^4G_{11/2}$	$3d^6\ (^3H)\ 4p\ z^4G_{9/2}$	−2.801		
4186.776	$3d^6\ 4d\ ^4D_{7/2}$	$3d^6\ (^3H)\ 4p\ z^4G_{9/2}$	−2.943		
4261.611	$3d^6\ 4d\ ^4G_{9/2}$	$3d^6\ (^3P)\ 4p\ y^4D_{7/2}$	−2.879		
4324.186	$3d^6\ 4d\ ^4G_{9/2}$	$3d^6\ (a^3F)\ 4p\ y^4F_{7/2}$	−2.513		
4354.334	$3d^6\ 4d\ ^4D_{7/2}$	$3d^6\ (a^3P)\ 4p\ y^4D_{7/2}$	−1.330		
4372.779	$3d^6\ 4d\ ^4G_{9/2}$	$3d^6\ (^3H)\ 4p\ z^2G_{7/2}$	−2.840		
4403.030	$3d^6\ 4d\ ^4G_{11/2}$	$3d^6\ (a^3F)\ 4p\ y^4F_{9/2}$	−2.102		
4435.209	$3d^6\ 4d\ ^6P_{7/2}$	$3d^6\ (a^3P)\ 4p\ y^4D_{7/2}$	−2.628		
4545.138	$3d^6\ 4d\ ^4D_{7/2}$	$3d^6\ (a^3P)\ 4p\ y^4D_{5/2}$	−2.540		
4598.486	$3d^6\ 4d\ ^4D_{7/2}$	$3d^6\ (a^3F)\ 4p\ x^4D_{7/2}$	−1.512		
4668.915	$3d^6\ 4d\ ^4D_{7/2}$	$3d^6\ (a^3F)\ 4p\ x^4D_{5/2}$	−2.638		
4688.779	$3d^6\ 4d\ ^6P_{7/2}$	$3d^6\ (a^3F)\ 4p\ x^4D_{7/2}$	−2.760		
4728.179	$3d^6\ 4d\ ^4G_{9/2}$	$3d^6\ (a^3F)\ 4p\ y^4G_{7/2}$	−2.753		
4780.018	$3d^6\ 4d\ ^4G_{11/2}$	$3d^6\ (a^3F)\ 4p\ y^4G_{9/2}$	−2.600		
4821.081	$3d^6\ 4d\ ^4D_{7/2}$	$3d^6\ (a^3F)\ 4p\ y^4G_{9/2}$	−2.916		
5129.745	$3d^6\ 4d\ ^4G_{9/2}$	$3d^6\ (^3G)\ 4p\ x^4G_{9/2}$	−2.814		
5192.438	$3d^6\ 4d\ ^4G_{9/2}$	$3d^6\ (^3G)\ 4p\ x^4G_{7/2}$	−2.101		
5214.489	$3d^6\ 4d\ ^4G_{9/2}$	$3d^6\ (^3G)\ 4p\ x^4F_{9/2}$	−2.632		
5215.760	$3d^6\ 4d\ ^4G_{11/2}$	$3d^6\ (^3G)\ 4p\ x^4G_{9/2}$	−1.614		
5264.689	$3d^6\ 4d\ ^4D_{7/2}$	$3d^6\ (^3G)\ 4p\ x^4G_{9/2}$	−2.853		
5303.394	$3d^6\ 4d\ ^4G_{11/2}$	$3d^6\ (^3G)\ 4p\ x^4F_{9/2}$	−1.542		
5315.561	$3d^6\ 4d\ ^4G_{9/2}$	$3d^6\ (^3G)\ 4p\ x^4F_{7/2}$	−1.464		
5353.989	$3d^6\ 4d\ ^4D_{7/2}$	$3d^6\ (^3G)\ 4p\ x^4F_{9/2}$	−2.479		
7859.171	$3d^6\ 4d\ ^4D_{7/2}$	$3d^6\ (^3D)\ 4p\ w^4P_{5/2}$	−1.635		
8126.627	$3d^6\ 4d\ ^6P_{7/2}$	$3d^6\ (^3D)\ 4p\ w^4P_{5/2}$	−2.850		

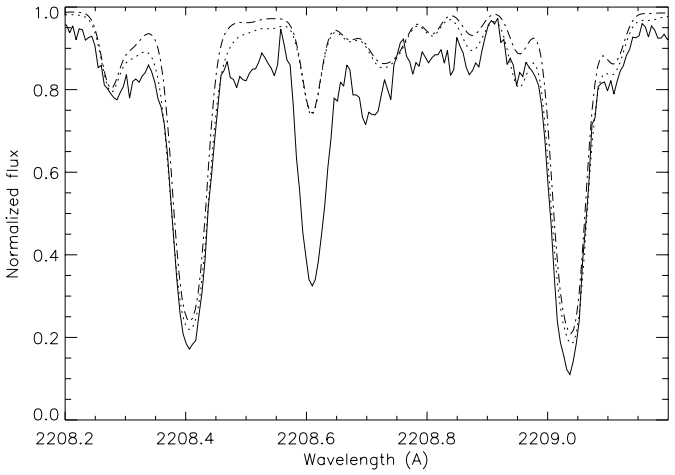

Fig. 6. The fitting of two Fe II lines at 2208.4 and 2209.0 Å in the GHRS spectrum of χ Lupi. The solid line is the observed stellar spectrum, the dashed line is the synthetic spectrum using our experimental values and the dotted line shows the synthetic spectrum giving the astrophysical log gf-value in Table 3.

observed in the laboratory, should be of the same quality, and justifies the inclusion of calculated values in Table 3. The deviation in Fig. 7 is about 10% for the stronger lines, but for weaker lines a larger scatter is seen, which might be due to a larger uncertainty in the calculations as well as in the measurements. It can also be noted that our calculated values are consistently smaller, on average by about 10%, than the experimental values. This might be due to an uncertainty in the theoretical value of the dipole operator or to a systematic error in the experimental lifetimes. The uncertainty given for the latter are of the order of 10%. In the comparison with Kurucz's data (Fig. 8) the agreement is still good, but the scatter is larger. Our conclusion is that where no experimental data are available Raassen's theoretical data for the 4p-4d transition array should be used in the calculation of stellar spectra. In order to test the significant difference found between the experimental and astrophysical log gf-values we have used all 4p-4d transitions we find in the observed GHRS spectrum of χ Lupi and derived astrophysical log gf-values. These are compared with our calculated data in Fig. 9. For most of the strong lines there is a clear discrepancy

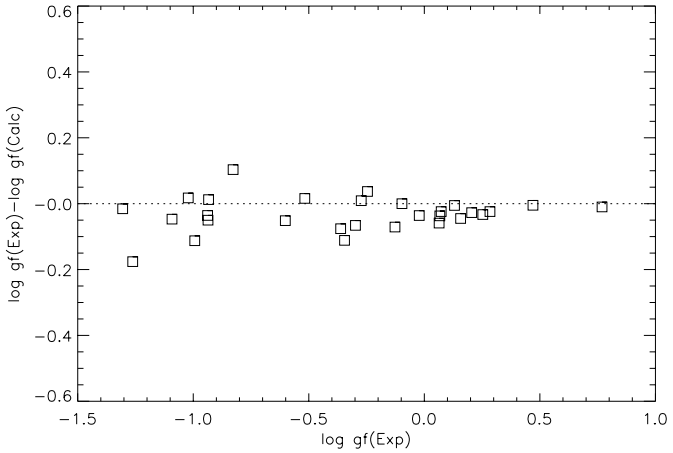

Fig. 7. The difference between the experimental and calculated log gf values reported in this paper (Table 2).

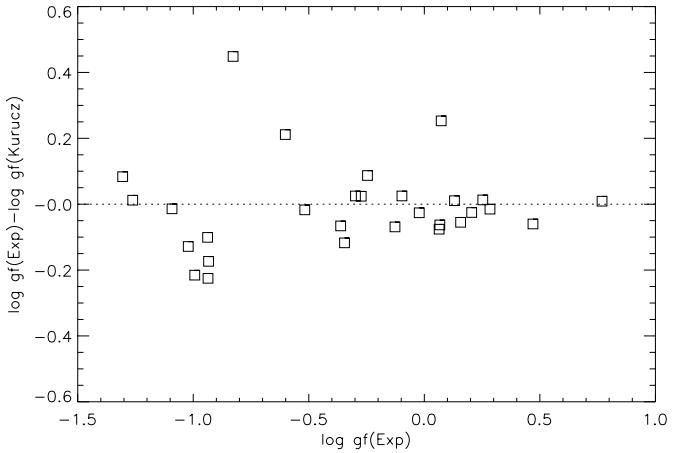

Fig. 8. The difference between our experimental log gf values and those calculated by Kurucz.

between experimental and astrophysical values, whereas there is a better agreement for the weaker lines.

6. Conclusion

We have measured absolute oscillator strengths for 29 lines of the $3d^6(^5D)4p$ -$3d^6(^5D)4d$ supermultiplet with an estimated accuracy of 12–22%. The data are compared to calculated values, showing a remarkably good agreement. The discrepancy between the experimental and theoretical values is within the measurement errors for 25 of the 29 lines, having a span of more than two orders of magnitude in strength. The larger discrepancy between the experimental data and Kurucz's data favors the use of Raassen's database for Fe II in calculation of stellar spectra. The missing opacity in the ultraviolet spectrum of χ Lupi in the features assigned to 4p-4d transitions of Fe II is most probably not due to deficiencies in the atomic data.

Acknowledgements. The authors would like to thank Drs. Ulf Litzén and Glenn Wahlgren for enlightening discussions. We (H.N. and C.M.S.) gratefully acknowledge grants from the Royal Physiographic Society in Lund. The FERRUM project is supported by the Swedish Natural Science Research Council.

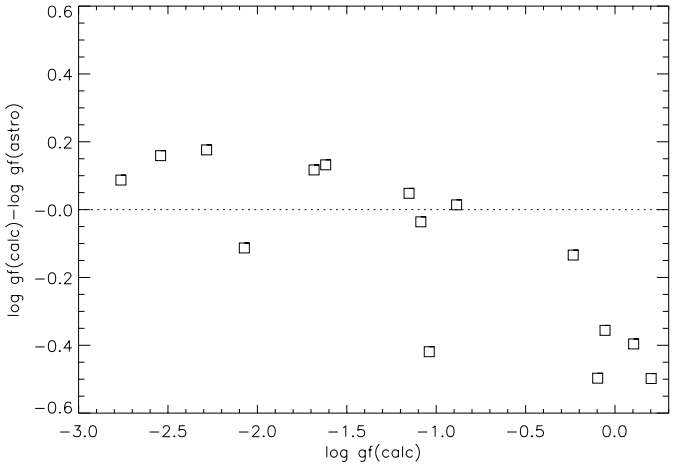

Fig. 9. The difference between the calculated and the astrophysical log gf values reported in this paper (Table 3).

References

Blom A., 2000, Lund Report on Atomic Physics, LRAP 262
Brandt J.C., Heap S.R., Beaver E.A., et al., 1999, AJ, 117, 1505
Brault J.W., Abrams M.C., 1989, In: High Resolution Fourier Transform Spectroscopy. OSA Technical Digest Series vol. 6, Optical Society of America, Washington, p. 110
Fuhr J.R., Martin G.A., Wiese W.L., 1988, J. Phys. Chem. Ref. Data 17, Suppl. 4
Hameed S.J., 1972, J. Phys. B 5, 746
Hansen J.E., Uylings P.H.M., Raassen A.J.J., 1988, Phys. Scr. 37, 664
Kurucz R.L., 1993, SYNTHE Synthesis Programs and Line Data. (Kurucz CD-ROM No. 18)
Laughlin C., 1992, Phys. Scr. 45, 238
Li Z.-S., Lundberg H., Sikström C.M., Johansson S., 1999, (Paper I) EPJ D 6 9
Leckrone D.S., Proffitt C.R., Wahlgren G.M., Johansson S.G., Brage T., 1999, ApJ 117, 1454
Parpia F.A., Froese Fischer C., Grant I.P., 1996, Comput. Phys. Commun. 94, 249
Raassen A.J.J., Uylings P.H.M., 1998a, A&A 340, 300
Raassen A.J.J., Uylings P.H.M., 1998b, J. Phys. B: At. Mol. Opt. Phys. 31, 3137
Siems A., Kock M., Johansson S., Litzén U., 1995, JQSRT 56 513
Sikström C.M., Schultz-Johanning M., Kock M., et al., 1999, J. Phys. B: At. Mol. Opt. Phys. 32, 5687
Wahlgren G.M., Adelman S.J., Robinson R.L., 1994, ApJ 434, 349